Macromolecules

Article

Cite This: Macromolecules 2019, 52, 2669−2680

pubs.acs.org/Macromolecules

# Structure and Mechanical Properties of Ethylene/1-Octene Multiblock Copolymers from Chain Shuttling Technology

Finizia Auriemma,*[,†] Claudio De Rosa,[†] Miriam Scoti,[†] Rocco Di Girolamo,[†] Anna Malafronte,[†] Massimo Christian D'Alterio,[†] Laura Boggioni,[‡] Simona Losio,[‡] Antonella Caterina Boccia,[‡] and Incoronata Tritto[‡]

[†]Dipartimento di Scienze Chimiche, Università di Napoli Federico II, Via Cintia, I-80126 Napoli, Italy

[‡]Istituto per lo Studio delle Macromolecole (ISMAC), Consiglio Nazionale delle Ricerche (CNR), Via E. Bassini 15, 20133 Milano, Italy



**ABSTRACT:** The mechanical properties and the structural transformations occurring during deformation of some commercial grades of ethylene/1-octene multiblock copolymers (OBCs) obtained from chain shuttling technology are analyzed. The samples are characterized by a statistical multiblock architecture, where soft and amorphous blocks with high octene concentration (≈18.9 mol %) alternate with hard and crystalline blocks with low octene concentration (≈0.5 mol %). The length of blocks (BL) and the number of blocks/chain (NB) change from chain to chain according to a statistical distribution. The selected samples have molecular mass in the range 85−130 kg/mol, percentage of hard segments in the range 15−27%, and a melting temperature of ≈120 °C. The average molecular masses of the hard blocks $M_H$ and soft blocks $M_S$ are in the ranges 2−3 kg/mol and 6−15 kg/mol, respectively, whereas the number of blocks/chain is in between 2 and 17. Even though the samples are characterized by similar octene concentration, small difference in molecular mass, and fractional content of hard blocks, they show remarkable differences of mechanical properties, depending on the average BL and NB values, encompassing from those of strong elastomers, in the case of samples with low block length and high number of blocks/chain, to those of soft elastomers, in the case of samples with high block length and low number of blocks/chain. The differences in the mechanical properties of OBC samples are amplified by stretching at high temperatures. Not previously stretched films obtained by compression molding show only partial recovery of the initial dimensions in mechanical cycles of stretching and releasing the tension, with values of recovered strain higher than 50% at 25 °C. However, the resultant specimens obtained by release of the tension show good elastomeric properties in a wide deformation range at 25 °C and, in the case of the samples with high strength, also at 60 °C. Fiber diffraction analysis reveals that by stretching at high deformation the orientation of the crystals is accomplished by mechanical melting and formation of an oriented amorphous phase, namely, involving the hard segments extracted from the crystals. Upon releasing the tension recrystallization occurs, and the high degree of orientation achieved by the crystals and amorphous phase is lost.

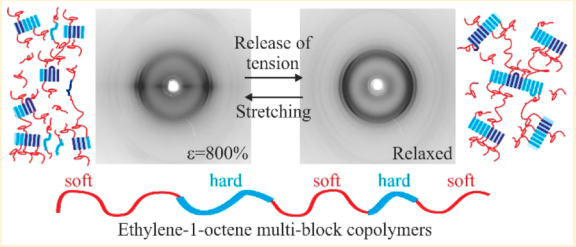


## INTRODUCTION

Olefin multiblock copolymers (OBC) synthesized by the Dow Chemical Company through the chain shuttling technology (CST)[1] and commercialized under the trade name INFUSE[2] are thermoplastic elastomers with interesting properties, as they join in the same material apparently conflicting properties, such as high melting temperature and low glass transition temperature coupled with low density, the presence of a pronounced $\alpha$ relaxation even at high average comonomer concentration and low degree of crystallinity, and good elastomeric properties even at high temperatures.[1,3−7] They are obtained from the copolymerization of ethylene with 1-octene in the presence of two organometallic catalysts with different capability toward incorporation of the two comonomers and a chain shuttling agent (CSA), which allows for the reversible transfer of growing chains between catalytic centers.[1,3,8−15] The resultant copolymer chains have a statistical multiblock architecture which consists in the alternation of crystallizable copolymer segments with low octene content defining the hard blocks H and elastomeric amorphous or poorly crystalline segments with high octene content defining the soft blocks S.[1] As the process is regulated by the probability of shuttling between identical or different catalytic centers, leading to the exchange of blocks of the same or different type, respectively, the chains of OBCs are nonuniform, as they include blocks with a statistical distribution of length (BL) and number of blocks/chain (NB).[1,8,10,11,13−15] In particular, not only the block length and the number of blocks/chain vary from chain to chain but also

Received: November 18, 2018
Revised: February 22, 2019
Published: March 18, 2019




DOI: 10.1021/acs.macromol.8b02470
Macromolecules 2019, 52, 2669−2680

the lengths of the blocks constituting each chain are nonuniform.

In general, for any fixed ratio of comonomers in the feed and reaction conditions (temperature, solvent, pressure, cocatalyst, etc.), the concentrations of octene units in the hard and soft blocks depend on the couple of selected organometallic catalysts, regardless of CSA concentration, if the propagation rates for monomers insertion on the growing chains are higher than the rates of chain shuttling reactions.[12] The average block length and the average number of blocks/chain along with the corresponding distributions, instead, depend on the relative amount of the catalysts, the corresponding propagation rates, CSA concentration, chain shuttling rates, and the possible use of hydrogen often included in the reaction protocol for molar mass regulation.[1,3,8−15] In practice, whereas molecular parameters such as molecular mass, molecular mass distribution, average comonomer concentration, comonomer concentration in the hard and soft blocks, and hence fractional block content may be easily determined resorting to standard characterization techniques,[4−7,16−26] details concerning the distribution of block length and number of block/chain are still not available because of intrinsic experimental difficulties in uncovering this kind of information, and even the corresponding average values are not yet defined.[15,27] In the lack of more quantitative information related to the values of these elusive parameters any attempt to establish structure−properties relationships for these systems can be deceptive.

The issue of a more quantitative approach for the determination of reliable values for the parameters BL and NB is challenging, also because CST enables synthesizing samples with identical average comonomer concentration and fractional block content, virtually characterized by any value for the average length and number of blocks/chain, and properties ranging from those of diblock copolymers to those of statistical copolymers. The interest for these systems relies in the possibility to widen the range of application of these novel materials at low cost, eventually designing molecular architectures endowed with properties that fall outside conventional applications.[3]

The structure, morphology, and mechanical properties of OBCs with different characteristics in terms of octene concentration in the hard and soft blocks and fractional content of hard blocks have been widely studied to date.[4−7,16−26] These studies have highlighted that the hard blocks tend to crystallize in the orthorhombic form of polyethylene (PE) forming well-organized lamellae, which melt at temperatures up to 50 °C higher than random copolymers with identical density. Upon crystallization, the soft blocks are rejected in separated domains.[4,16,18,23,24] The crystalline lamellae in turn are organized in space-filling spherulites, suggesting that crystallization possibly takes place from a miscible melt.[4−7,16−25] Compared to random copolymers with similar density, the analysis of mechanical properties of OBCs reveals that at 25 °C, for both systems, the values of Young modulus are essentially controlled by the degree of crystallinity, and both show strain hardening and high ductility, the onset of strain hardening, and breaking occurring at higher deformations for OBCs.[4−7,17,24,25] At higher temperature both systems show a decrease of Young modulus and no strain hardening, but whereas in the case of random copolymers this is due to melting or partial melting of crystals, in the case of OBCs this can be attributed to activation of the crystalline $\alpha$ relaxation.[5−7] The OBC samples also show higher elastic recovery upon release of the tension from specimens stretched at high deformations.[5−7,24,25] All in all, the resultant specimens obtained by releasing the tension of stretched films at high deformation show good elastomeric properties in a rather high deformation range, at low and high temperatures.[5−7,17,24,25] The role of possible phase separation on the crystallization of hard blocks in the case of OBCs samples characterized by different segregation strength between the blocks has been also studied,[18−22] finding that the mechanical properties of OBCs samples crystallized from homogeneous melt are better than those of samples crystallized from the phase-separated melt.[23,24]

Small and/or large differences in the crystallization and mechanical properties of OBCs in terms of differences in the values of average block length and number of blocks/chain have never been assessed to date, and the role of these parameters has been only qualitatively inferred to discuss experimental trends. In a recent study,[28] we have proposed an empirical approach to establish reliable values for these parameters. The method relies on the results of SAXS analysis of melt-crystallized samples obtained at fast cooling rates, which indicate that the hard blocks of OBCs tend to crystallize in separated domain, forming lamellar stacks with little or no inclusion of soft blocks in the interlamellar regions.[28] According to this method, reliable values for the average molecular mass of hard blocks $M_H$ can be obtained from the values of lamellar parameters extracted from SAXS measurements, considering that the values of long spacing $L$ and thickness of amorphous layers $l_a$ scale as the square root of the mean-square gyration radius of the chains in the unperturbed state,[29] $R_g \approx M_H^{1/2}$, according to a linear relationship set up by Rault and co-workers[30] in the case of polyethylene. The method is based on the simple consideration that under fast cooling rates the gyration radius of the chains at high temperatures does not change in the undercooled melt if crystallization takes place at a high rate.[30] Under these circumstances, chains have no time to relax and/or disentangle, so that for lamellar crystals growing at high rate and placed at separation distance $L \approx R_g$, distinct crystallizable segments belonging to the same chain have a high probability to be included in lamellar crystals placed at distance $L \approx R_g$ as they have no time to relax.[29,30] For sufficiently high crystallization rates, the relaxation of the portions of chains located in the amorphous regions connecting the lamellar crystals is hampered, and the state of the amorphous phase and the entanglement density are frozen in nonequilibrium conditions.[29,30] The scaling of the lamellar parameters $L$ and $l_a$ with $R_g$ and hence $M_H$ is the result of the balance between the energy penalty associated with the nonequilibrium state of the chain in the interlamellar amorphous layers and the enthalpic gain associated with crystallization.[30] From the values of $M_H$, the values of average molecular mass of a diblock HS repetition unit $M_{HS}$ including consecutive hard (average molecular mass $M_H$) and soft segments (average molecular mass $M_S$) and of soft blocks in a HS repetition unit are straightforwardly calculated as $M_{HS} = M_H w_H^{-1}$ with $w_H$ the average fraction of hard blocks and $M_S = M_{HS} - M_H$.[28] The average number of blocks/chain NB is finally calculated as a quantity in between $n_1 = M_n M_{HS}^{-1}$ and $n_2 = M_w M_{HS}^{-1}$, where $M_n$ and $M_w$ are the number- and mass-average molecular mass of the OBC samples, respectively.[28]

It is worth noting that even though the so-determined values of $M_H$ and $M_S$ are affected by a systematic error, a preliminary



DOI: 10.1021/acs.macromol.8b02470
Macromolecules 2019, 52, 2669−2680

**Table 1. Main Properties of OBC Multiblock Samples**

| sample | density ($g/cm^3$)[a] | (%)[b] | $M_w$ (kg/mol)[c] | $M_w/M_n$[c] | O (mol %)[d] | $w$(O) (wt %)[d] | $w_H$[e] | $T_m$ (°C)[f] | $T_c$ (°C)[f] | $T_g$ (°C)[f] | $x_c$ (%)[g] | $M_H$ (kg/mol)[h] | $M_S$ (kg/mol)[h] | $M_{HS}$ (kg/mol)[h] | $[HM_H\text{-}SM_S]_{n_1/n_2}$ of HS repetition unit |
|---|---|---|---|---|---|---|---|---|---|---|---|---|---|---|---|
| EO-130 | 0.877 | | 130 | 2.1 | 12.3 | 35.9 | 0.27 | 121 | 97 | ≈−60 | 17 (63) | 2.3 | 6.2 | 8.4 | $[H2\text{-}S6]_{7/15}$ |
| EO-130Es | | 8.1 | 82 | 2.3 | 20.1 | 50.2 | ≈0 | 46 | 10 | ≈−60 | | | | | |
| EO-130Ei | | 91.9 | 151 | 1.8 | 12.4 | 36.2 | 0.26 | 120 | 103 | ≈−60 | 18 (69) | 2.3 | 6.5 | 8.8 | $[H2\text{-}S6]_{10/17}$ |
| EO-129[k] | 0.866 | | 129 | 1.9 | 15.0 | 41.4 | 0.15 | 119 | 94 | ≈−60 | 9 (60) | 2.7 | 15.5 | 18.2 | $[H3\text{-}S15]_{4/7}$ |
| EO-129Es | | 14.1 | 96 | 1.9 | 18.8 | 48.1 | <0.01 | 46 | 10 | ≈−60 | | | | | |
| EO-129Ei | | 85.9 | 173 | 1.6 | 15 | 41.4 | 0.15 | 120 | 98 | ≈−6 | 11 (73) | 2.7 | 15.5 | 18.2 | $[H3\text{-}S15]_{6/9}$ |
| EO-115 | 0.877 | | 115 | 1.9 | 13.0 | 37.5 | 0.23 | 122 | 96 | ≈−60 | 14 (61) | 2.3 | 7.6 | 9.9 | $[H2\text{-}S8]_{6/12}$ |
| EO-115Es | | 6.2 | 82 | 2.2 | 18.6 | 47.8 | <0.01 | 42 | 16 | ≈−60 | | | | | |
| EO-115Ei | | 93.8 | 144 | 1.9 | 13.1 | 37.7 | 0.23 | 121 | 104 | ≈−60 | 15 (65) | 2.3 | 7.6 | 9.9 | $[H2\text{-}S8]_{8/15}$ |
| EO-107 | 0.877 | | 107 | 2.0 | 12.4 | 36.1 | 0.26 | 124 | 99 | ≈−60 | 17 (65) | 3.2 | 9.2 | 12.4 | $[H3\text{-}S9]_{4/9}$ |
| EO-107Es | | 9.1 | 66 | 2.3 | 18.6 | 47.8 | <0.01 | 42 | 18 | ≈−60 | | | | | |
| EO-107Ei | | 90.9 | 114 | 2.0 | 12.6 | 36.6 | 0.25 | 123 | 108 | ≈−6 | 19 (75) | 3.2 | 9.7 | 12.9 | $[H3\text{-}S10]_{4/9}$ |
| EO-85[k] | 0.877 | | 85 | 3 | 12.5 | 36.4 | 0.26 | 123 | 102 | ≈−60 | 16 (65) | 3.0 | 8.5 | 11.4 | $[H3\text{-}S8]_{2/7}$ |
| EO-85Es | | 12.4 | 40 | 4.8 | 19.1 | 48.6 | ≈0 | 64 | 18 | ≈−60 | <2 | | | | |
| EO-85Ei | | 87.6 | 90 | 3 | 12.8 | 37.0 | 0.25 | 121 | 113 | ≈−60 | 18 (74) | 3.0 | 8.9 | 11.9 | $[H3\text{-}S9]_{3/8}$ |

[a]From technical sheets of the commercial grades. [b]Amounts of ether soluble (Es) and insoluble (Ei) fractions. [c]Mass average molecular mass and polydispersity index from GPC analysis as described in ref 28. [d]Total concentration of octene units in mol % and wt % from solution $^{13}C$ NMR analysis as described in ref 28. Data are affected by ≈2% relative error. [e]Weight fraction of hard blocks calculated as $w_H = (0.48 - w(O))/0.46$, with $w(O)$ the average weight fraction of octene units in the sample. [f]From DSC analysis of melt-crystallized samples.[28] [g]Total average crystalline index, determined from WAXS profiles of melt-crystallized samples. Number in parentheses are relative to the sole hard blocks ($x_c/w_H$). [h]Calculated according to the method of ref 28. [k]The pellets are covered by talc at surface.



DOI: 10.1021/acs.macromol.8b02470
Macromolecules 2019, 52, 2669−2680

account demonstrates that they may be considered a good approximation of the true values as they can help to explain the properties OBCs at the molecular level.[28]

In this paper the mechanical properties and the structural transformations occurring during deformation of some commercial grades of OBCs are analyzed in detail. This study completes and extends the analysis performed in ref 28 on the same kinds of samples. The samples are characterized by hard and soft blocks with identical concentration of comonomeric units, equal to ≈0.5 and ≈18.9 mol %, respectively, small difference in molecular mass and fractional content of hard blocks, and subtle differences in the melting and crystallization properties but remarkable differences for the mechanical properties. We highlight that the mechanical properties of these systems reflect the differences in the average molecular mass of soft and hard blocks and number of blocks/chain, establishing the validity of our method for the calculation of these parameters and the advantage of the approach to understand the material properties at the molecular level.

## EXPERIMENTAL PART

The ethylene/1-octene block copolymers were supplied by the Dow Chemical Company as pellets. The octene concentration in the hard and soft blocks are ≈0.5 and 18.9 mol %, (≈2 and 48.3 wt %), respectively. The molecular mass, the average concentration of octene units, the fraction of hard blocks, the melting temperature, and crystallinity index of the melt-crystallized samples are shown in Table 1. Exhaustive extraction with boiling diethyl ether ($Et_2O$) in a Kumagawa extractor indicates that all samples include a small amount (6−14 wt %) of an ether-soluble fraction (*Es*). The average molecular mass of the hard ($M_H$) and soft blocks ($M_S$) in a HS repetition unit, as determined from SAXS analysis with the method of ref 28, is also reported.

Here in the following, the samples are designed with the name EO-*x*, where *x* specifies the mass average molecular mass in kg/mol. The corresponding ether-soluble (Es) and ether-insoluble (Ei) fractions are instead indicated as EO-*x*Es and EO-*x*Ei, respectively.

Films of uniform thickness (≈500 μm) were prepared by compression molding in a press. The samples (200−300 mg) were sandwiched between two flat brass foils and heated between the plates of the press up to ≈150 °C. After 10 min isotherm at 150 °C, the samples were cooled to 25 °C (average cooling rate ≈30 °C/min). We have checked that no preferred orientation was induced in the samples by effect of the molding process.

X-ray powder diffraction profiles were collected in reflection geometry with a diffractometric apparatus Empyrean (PANalytical) using Ni-filtered Cu K$\alpha$ radiation ($\lambda$ = 0.15418 nm). Fiber diffraction data were collected on an imaging plate and processed with a digital imaging reader (PerkinElmer Cyclone Plus Phosphor Imager) mounted in a cylindrical camera (Ni-filtered Cu K$\alpha$ radiation).

The crystallinity index was evaluated from the X-ray powder diffraction profiles, after subtraction for background intensity, as the ratio $x_c = A_c/A_t$, where $A_c$ is the diffraction area due to the crystalline phase and $A_t$ is the total area subtending the diffraction profile. The value of $A_c$ was determined by subtracting the contribution from the amorphous phase $A_a$ from $A_t$ ($A_c = A_t - A_a$). The contribution from the amorphous phase was determined by measuring the X-ray data of the samples in the melt state in the temperature range 140−160 °C. The profiles recorded at 140 °C were then horizontally translated up to have the maximum at ≈19°, coincident with the extrapolated $2\theta$ position of the amorphous phase at 25 °C, and scaled in the *y*-coordinate.

Stress−strain curves and hysteresis cycles were recorded according to the standard test method ASTM D882-83 using a mechanical test machine Zwicky (by Zwick Roell) equipped with a temperature-controlled chamber at 25 and 60 ± 1 °C. Tests were performed on stripes of free length $L_0$ = 10 mm and width $w_0$ = 5 mm, cut from compression molded films (thickness 0.5 mm). They were stretched up to breaking or up to a final length $L_f$ (corresponding maximum deformation $\varepsilon_{max} = 100 \times (L_f - L_0)/L_0$). To measure elongation, benchmarks were drawn on the specimens. Hysteresis cycles were performed on specimens obtained by releasing the tension from $\varepsilon_{max}$ of compression-molded films by measuring the stress−strain curves during consecutive cyclic tests made up of a stretching step followed by a relaxation step, at controlled deformation rate. In practice, stretch-relaxed specimens were prepared by stretching not previously oriented specimens (initial length $L_0$) up to a maximum deformation $\varepsilon_{max}$ (final length $L_f$) and then releasing the tension. In the hysteresis cycles, stretch-relaxed specimens of new initial length $L_i$ coincident with the length $(L_r)_{i-1}$ achieved by the sample 10 min after end of the preceding cycle ($L_r$ standing for the length of stretch-relaxed sample) were repeatedly stretched up to the same final length $L_f$, that is, reaching the maximum deformation $\varepsilon_{max}$ achieved in the preparative step. The tension set $(t_s)_i$, corresponding to the permanent deformation experienced by the sample after the *i*-th cycle, was calculated as $(t_s)_i = [((L_r)_i - L_i)/L_i] \times 100$, where *Li* and $(L_r)_i$ are the initial and the relaxed length of the specimen at the beginning and 10 min after the end of the *i*th cycle. The percentage of dissipated energy $(W_{diss})_i$ for each cycle was also calculated as the hysteresis area. Finally, for the specimens prepared by stretching the initial unstretched films up to $\varepsilon_{max}$ and then releasing the tension, the percentage of recovered strain $R(\varepsilon_{max})$ and the values of elastic recovery $r(\varepsilon_{max})$ were also calculated as $R(\varepsilon_{max}) = 100 \times [(L_f - (L_r)_0)/[(L_f - L_0)]$ and $r(\varepsilon_{max}) = [(L_f - (L_r)_0)/(L_r)_0] \times 100$, respectively, where $(L_r)_0$ is the length of the specimen measured 10 min after release of the tension.

Tests were performed at deformation speed $v = kL_0$ with $k$ = 10 $min^{-1}$ for the rupture tests, $k$ = 0.1 $min^{-1}$ for the measures of Young modulus, and $k$ = 10 $min^{-1}$ for recording the hysteresis cycles. All tests were averaged over a minimum of five independent curves.

## RESULTS AND DISCUSSION

As shown in Table 1, the selected set of unfractionated samples have mass average molecular mass spreading in the range 85−130 kg/mol, polydispersity index close to 2 (3 for the sample EO-85), average octene concentration in between 36 and 41 wt % (12−15 mol %), and mass fraction of hard segments $w_H$ comprised between 0.15 and 0.27. After fractionation with diethyl ether, the ether-insoluble factions (Ei) show similar octene concentration to that of the unfractionated samples, and only the molecular mass results slightly higher. The ether-soluble fractions of all samples (Es), which correspond to only 6−14 wt % of the total, instead show octene concentration of 19−20 mol %, similar to that of soft blocks, mass average molecular mass 50−70% lower, and polydispersity index slightly higher than those of the unfractionated samples.

The values of the average molecular mass of the hard ($M_H$) and soft ($M_S$) blocks in a HS repetition unit and of the average mass of a HS repetition unit $M_{HS}$ (= $M_H$ + $M_S$) of the unfractionated OBC samples are also reported in Table 1, as evaluated in ref 28 from SAXS data using an empirical equation.[30] The samples are identified with the dub $[HM_H - SM_S]_{n_1/n_2}$ where the subscripts $n_1$ and $n_2$ specify the average number of blocks/chain, evaluated as $n_1 = M_n M_{HS}^{-1}$ and $n_2 = M_w M_{HS}^{-1}$. This approach is here extended also to the sample EO-129 and to the Ei fractions. It is apparent that the values of $M_H$ and $M_S$ in the case of the Ei fractions are similar to those of the unfractionated samples (Table 1), whereas the average number of blocks/chain $n_1$ and $n_2$ in the Ei fractions results slightly higher, in agreement with the higher molecular mass. The information in the dub $[HM_H - SM_S]_{n1/n2}$ allows differentiating OBC samples with apparently small difference


DOI: 10.1021/acs.macromol.8b02470
Macromolecules 2019, 52, 2669−2680

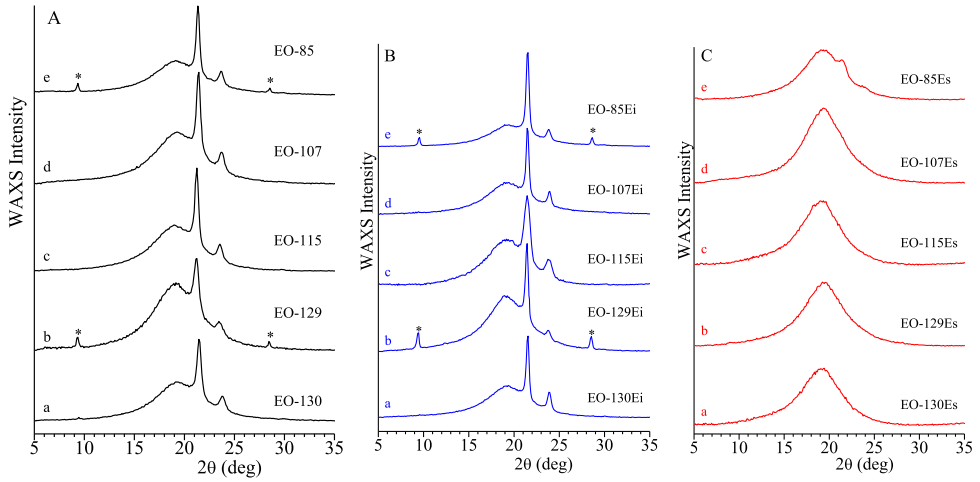


**Figure 1.** X-ray powder diffraction profiles of OBC samples (A) and of the corresponding ether-soluble Es (C) and ether-insoluble Ei (B) fractions obtained by compression molding. Stars in A and B indicate the diffraction peaks of talc used as additive to prevent the cohesion of pellets.

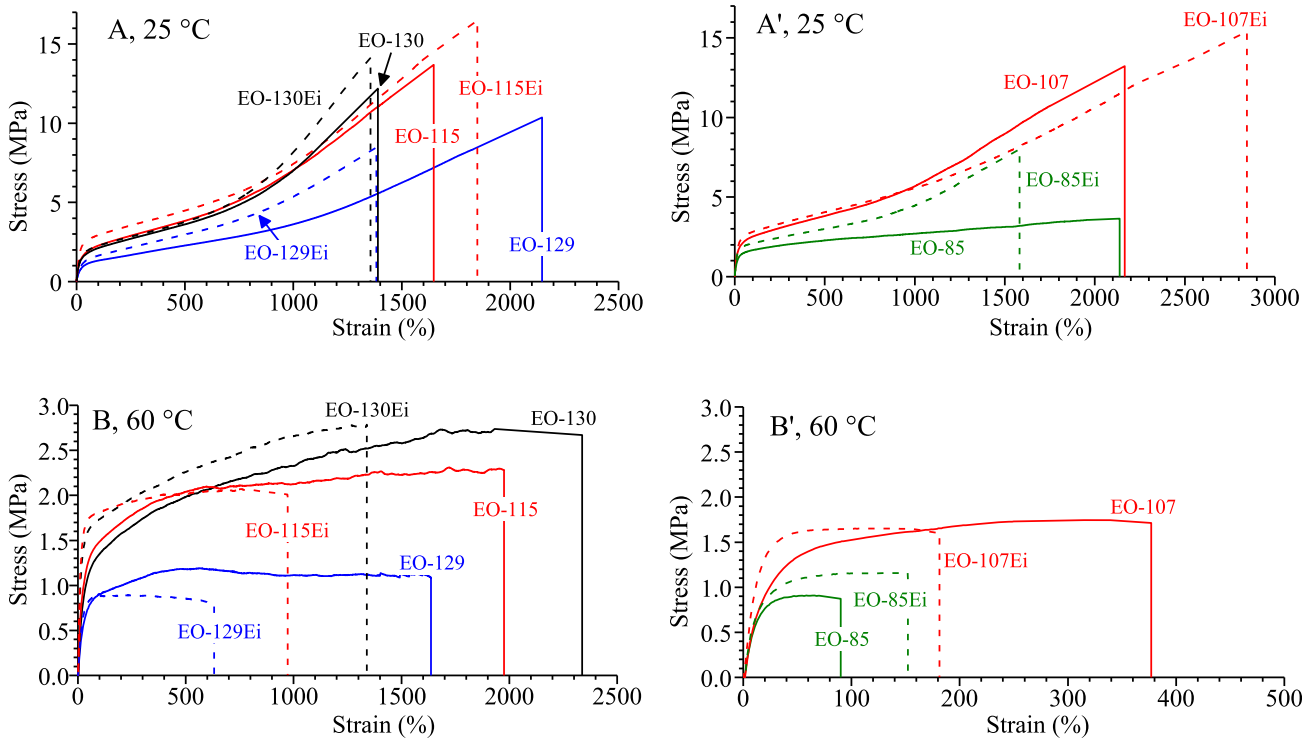


**Figure 2.** Stress−strain curves (nominal values) of the unfractionated OBC samples (continuous lines) and of the corresponding ether insoluble fractions (dashed lines) obtained by compression molding from the melt, recorded at 25 °C (A, A′) and 60 °C (B, B′).

in the concentration of octene units and fractional amount of hard blocks and highlights the analogies. In particular, the samples EO-130 and EO-115 and the corresponding Ei fractions show only small differences as far the average molecular mass of the hard ($M_H \approx 2$ kg/mol) and soft blocks ($M_S \approx 6-8$ kg/mol) are concerned. They include, on average, from 6 to 17 blocks/chain. These samples show the shortest block length and the highest number of blocks/chain. Also, the samples EO-107 and EO-85 and the corresponding Ei fractions appear similar, as they correspond to values of $M_H$ close to 3 kg/mol and $M_S$ in the range 8−10 kg/mol. Compared to the sample EO-130 and EO-115, these samples show a higher average molecular mass for the HS repetition units ($M_{HS}$). Moreover, because of their lower molecular mass, the samples EO-107 and EO-85 show a number of blocks/chain comprised in between 2 and 9, which is the lowest within the analyzed series. Finally, the sample EO-129 and the corresponding Ei fraction show average molecular mass of hard blocks $M_H$ of 3 kg/mol, similar to that of the samples E-107 and EO-85, but a much higher average molecular mass of the soft blocks ($M_S \approx$ 15 kg/mol) and a number of blocks/chain in the range 4−9. Therefore, the sample EO-129 shows the highest average block length for the HS repetition unit, but still a high number of blocks/chain, on average.

The X-ray powder diffraction profiles of OBC samples and of the corresponding ether-soluble (Es) and ether-insoluble (Ei) fractions are reported in Figure 1. The Ei fractions (Figure 1B) show diffraction profiles similar to those of the



DOI: 10.1021/acs.macromol.8b02470
Macromolecules 2019, 52, 2669−2680

Table 2. Young Modulus ($E$), Strain ($\varepsilon_y$), and Stress ($\sigma_y$) at Yield; Strain ($\varepsilon_b$), Stress ($\sigma_b$), and Tension Set ($t_b$) at Break of Unfractionated OBC Samples and of the Corresponding Ether-Insoluble Fractions Evaluated from Tensile Tests at 25 and 60 °C, Concentration of Octene Units (O), Weight Fraction of Hard Blocks ($w_H$) and Crystallinity ($x_c$)

| sample | | O (mol %) | $w_H$ (wt %) | $x_c$(WAXS) (%) | $\varepsilon_y$ (%) | $\sigma_y$ (MPa) | $\varepsilon_b$ (%) | $\sigma_b$ (MPa) | $t_b$ (%) | $E$ (MPa) |
|---|---|---|---|---|---|---|---|---|---|---|
| | | | | | Temperature 25 °C | | | | | |
| EO-130 | $[H2\text{-}S6]_{7/15}$ | 12.3 | 0.27 | 17 | 14 ± 2 | 1.8 ± 0.2 | 1400 ± 200 | 12 ± 3 | 380 ± 80 | 15 ± 2 |
| EO-130Ei | $[H2\text{-}S6]_{10/17}$ | 12.4 | 0.26 | 18 | 14 ± 4 | 1.8 ± 0.5 | 1400 ± 60 | 14 ± 1 | 250 ± 20 | 16 ± 1 |
| EO-129 | $[H3\text{-}S15]_{4/7}$ | 15.0 | 0.15 | 9 | 12 ± 2 | 1.2 ± 0.2 | 2100 ± 300 | 10 ± 2 | 170 ± 10 | 6 ± 1 |
| EO-129Ei | $[H3\text{-}S15]_{6/9}$ | 15.0 | 0.15 | 11 | 17 ± 3 | 1.4 ± 0.1 | 1400 ± 70 | 8 ± 2 | 84 ± 17 | 7 ± 1 |
| EO-115 | $[H2\text{-}S8]_{6/12}$ | 13.0 | 0.23 | 14 | 17 ± 3 | 1.9 ± 0.1 | 1600 ± 100 | 13 ± 1 | 190 ± 10 | 13 ± 1 |
| EO-115Ei | $[H2\text{-}S8]_{8/15}$ | 13.1 | 0.23 | 15 | 16 ± 2 | 2.6 ± 0.3 | 1800 ± 100 | 17 ± 2 | 200 ± 20 | 15 ± 1 |
| EO-107 | $[H3\text{-}S9]_{4/9}$ | 12.4 | 0.26 | 17 | 24 ± 5 | 2.4 ± 0.3 | 2200 ± 200 | 13 ± 2 | 260 ± 20 | 15 ± 2 |
| EO-107Ei | $[H3\text{-}S10]_{4/9}$ | 12.6 | 0.25 | 19 | 20 ± 4 | 2.5 ± 0.3 | 2800 ± 400 | 15 ± 2 | 390 ± 70 | 16 ± 3 |
| EO-85 | $[H3\text{-}S8]_{2/7}$ | 12.8 | 0.24 | 16 | 19 ± 2 | 1.6 ± 0.1 | 2100 ± 200 | 4 ± 1 | 400 ± 50 | 15 ± 1 |
| EO-85Ei | $[H3\text{-}S9]_{3/8}$ | 12.8 | 0.24 | 18 | 18 ± 2 | 1.9 ± 0.1 | 1600 ± 200 | 8.0 ± 0.5 | 250 ± 50 | 19 ± 2 |
| | | | | | Temperature 60 °C | | | | | |
| EO-130 | $[H2\text{-}S6]_{7/15}$ | 12.3 | 0.27 | 17 | 26 ± 1 | 1.3 ± 0.1 | 2300 ± 300 | 3.0 ± 0.2 | 400 ± 100 | 6 ± 1 |
| EO-130Ei | $[H2\text{-}S6]_{10/17}$ | 12.4 | 0.26 | 18 | 18 ± 6 | 1.6 ± 0.1 | 1400 ± 70 | 3.0 ± 0.2 | 400 ± 60 | 7 ± 1 |
| EO-129 | $[H3\text{-}S15]_{4/7}$ | 15.0 | 0.15 | 9 | 28 ± 2 | 0.8 ± 0.1 | 1700 ± 100 | 1.0 ± 0.2 | 610 ± 70 | 2.9 ± 0.3 |
| EO-129Ei | $[H3\text{-}S15]_{6/9}$ | 15 | 0.15 | 11 | 74 ± 9 | 1.0 ± 0.1 | 700 ± 100 | 0.8 ± 0.1 | 420 ± 20 | 2.9 ± 0.5 |
| EO-115 | $[H2\text{-}S8]_{6/12}$ | 13.0 | 0.23 | 11 | 26 ± 2 | 1.4 ± 0.1 | 2000 ± 200 | 2.2 ± 0.3 | 1000 ± 100 | 4.4 ± 0.9 |
| EO-115Ei | $[H2\text{-}S8]_{8/15}$ | 13.1 | 0.23 | 12 | 16 ± 1 | 1.4 ± 0.1 | 1000 ± 200 | 2.2 ± 0.2 | 400 ± 80 | 6.2 ± 0.2 |
| EO-107 | $[H3\text{-}S9]_{4/9}$ | 12.4 | 0.26 | 17 | 12 ± 3 | 1.4 ± 0.2 | 400 ± 50 | 1.7 ± 0.2 | 110 ± 40 | 7 ± 1 |
| EO-107Ei | $[H3\text{-}S10]_{4/9}$ | 12.6 | 0.25 | 19 | 17 ± 4 | 1.6 ± 0.2 | 180 ± 20 | 1.6 ± 0.1 | 45 ± 20 | 7 ± 1 |
| EO-85 | $[H3\text{-}S8]_{2/7}$ | 12.8 | 0.24 | 16 | 11 ± 1 | 0.8 ± 0.1 | 90 ± 20 | 0.9 ± 0.1 | 40 ± 10 | 6 ± 1 |
| EO-85Ei | $[H3\text{-}S9]_{3/8}$ | 12.8 | 0.24 | 18 | 11 ± 6 | 1.0 ± 0.5 | 150 ± 40 | 1.1 ± 0.1 | 34 ± 5 | 11 ± 2 |

unfractionated samples (Figure 1A), characterized by the presence of the 110 and 200 reflections of the orthorhombic form of polyethylene (PE) at $2\theta \approx 21°$ and 24° due to crystallization of the hard blocks, overlaying an amorphous halo centered at $2\theta \approx 19°$. The values of crystallinity index $x_c$ evaluated from the diffraction profiles are in the range 9−18%, and increase with increasing the fractional content of hard blocks $w_H$. After normalization for the fractional content of hard blocks ($x_c/w_H$), values of crystallinity index in the range 60−74% are achieved. The ether-soluble fractions show no apparent crystallinity (Figure 1C), and only for the sample EO-85 the Es fraction displays two small and broad reflections at $2\theta \approx 21°$ and 24° of the orthorhombic form of PE.

DSC analysis (data not shown) reveals that the melting temperatures of the unfractionated samples and the Ei fractions are in all cases around 120 °C, whereas the crystallization temperatures are spread in a rather wide range comprised between 94 and 113 °C (Table 1), the crystallization temperatures of the unfractionated samples being systematically lower by 4−11 °C than those of the corresponding Ei fractions. This indicates that the amorphous and/or poorly crystalline Es fractions act as a diluent delaying the crystallization of the hard blocks in the unfractionated samples. All the Es fractions show some level of crystallinity as they present faint melting and crystallization peaks at 40−60 and 10−20 °C, respectively. Finally, all the samples show a broad glass transition at nearly −60 °C (Table 1). The small crystallinity of the Es fractions indicates that the Es fractions include not only soft segments not attached to hard blocks but also soft segments attached to very short hard (crystallizable) segments, even though crystallization of long ethylene sequences belonging to the soft segments may not be excluded.

The stress−strain curves (nominal values) of unfractionated OBC samples and the corresponding ether-insoluble fractions are shown in Figure 2, whereas the mechanical parameters evaluated from the stress−strain curves are reported in Table 2. The samples were tested at 25 and 60 °C. The tensile properties of the Es fractions could not be measured as they are sticky and doughy and are subjected to flow upon handling, even at 25 °C. All the unfractionated samples and Ei fractions show only small differences in mechanical properties at 25 °C (Figure 2A,A′). They behave as strong elastomers, presenting values of deformation at break higher than 1300%, values of Young modulus higher than 13 MPa, and strain hardening at high deformations. A different behavior is observed for the samples EO-129, which presents lower values of Young modulus of ≈6−7 MPa in the unfractionated and fractionated samples, in agreement with the lower content of hard blocks, and for the unfractionated sample EO-85 that breaks at high deformation without strain hardening. In all cases, the mechanical properties of the unfractionated samples are not greatly altered upon removal of the ether-soluble fractions, in agreement with the fact that the relative amount of this fraction is small (below 14 wt %), and only a small increase of stiffness and/or strength generally coupled with some decrease of ductility is observed.

The differences in mechanical properties of the OBC samples become remarkably greater at 60 °C (Figure 2B,B′). In general, at 60 °C, that is, at a temperature still far from melting at 120 °C, the samples become softer and show no strain hardening, high ductility, and values of the Young modulus 2−3 times lower than those at 25 °C. Differences have been observed in the case of the samples EO-107 and EO-85, which, before and after removal of the ether-soluble fractions, show at 60 °C values of deformation at break remarkably lower (by a factor 10−20) than those at 25 °C, whereas the samples EO-130, EO-115, and EO-129 and the corresponding Ei fractions keep a high ductility.

The mechanical tests performed at 25 and 60 °C highlight different mechanical behavior due to differences in the average



DOI: 10.1021/acs.macromol.8b02470
Macromolecules 2019, 52, 2669−2680

Table 3. Values of Tension Set ($t_s$) and Dissipated Energy ($W_{diss}$) Evaluated from the Stress−Strain Curves Recorded during Hysteresis Cycles Performed at the Temperatures $T$ = 25 and 60 °C, of Stretch-Relaxed Specimens of the Samples OBC Prepared by Stretching at the Temperatures $T$ of Not Previously Oriented Films, Obtained by Compression Molding, Up to the Deformations $\varepsilon_{max} \approx 500$ and ≈1000% and Removing the Tension; Tension Set ($t_s(\varepsilon_{max})$), Elastic Recovery ($r(\varepsilon_{max})$), and Percentage of Recovered Strain ($R(\varepsilon_{max})$) Measured after Stretching of the Films Obtained by Compression Molding

| | | | $\varepsilon_{max} \approx 500\%$ | | | | | | | |
|---|---|---|---|---|---|---|---|---|---|---|
| sample | O (mol %) | $T$ (°C) | $t_s(500)$ (%) | $r(500)$ (%) | $R(500)$ (%) | $t_s^{I}(500)$ (%)[a] | $t_s^{II}(500)$ (%)[a] | $t_s^{III}(500)$ (%)[a] | $W_{diss}^{I}$ (%)[a] | $W_{diss}^{II}$ (%)[a] |
| EO-130 $[H2\text{-}S6]_{7/15}$ | 12.4 | 25 | 94 ± 9 | 208 ± 14 | 81 ± 12 | 22 ± 3 | 3.3 ± 0.3 | 1.9 ± 0.2 | 58.7 ± 1.1 | 49.3 ± 0.4 |
| | | 60 | 240 ± 9 | 80 ± 6 | 52 ± 3 | 1 ± 0.4 | 1 ± 0.3 | 1 ± 0.3 | 36 ± 2 | 36 ± 2 |
| EO-129 $[H3\text{-}S15]_{4/7}$ | 15 | 25 | 43 ± 3 | 320 ± 9 | 91 ± 19 | 29 ± 4 | 3.1 ± 0.1 | 1.8 ± 0.1 | 49 ± 1 | 37 ± 1 |
| | | 60 | 120 ± 6 | 160 ± 11 | 76 ± 7 | 2 ± 1 | 2 ± 1 | 2 ± 1 | 34 ± 1 | 30 ± 1 |
| EO-115 $[H2\text{-}S8]_{6/12}$ | 13.1 | 25 | 106 ± 3 | 191 ± 4 | 79 ± 3 | 14 ± 2 | 2.6 ± 0.2 | 1.5 ± 0.2 | 55.3 ± 0.8 | 47.8 ± 0.2 |
| | | 60 | 140 ± 4 | 150 ± 5 | 72 ± 3 | 1.0 ± 0.4 | 1.0 ± 0.5 | 1.0 ± 0.5 | 41 ± 2 | 37 ± 2 |
| EO-107 $[H3\text{-}S9]_{4/9}$ | 12.6 | 25 | 122 ± 8 | 170 ± 9 | 76 ± 6 | 12.7 ± 1.3 | 2.4 ± 0.4 | 1.3 ± 0.2 | 58.2 ± 0.3 | 50.9 ± 0.2 |
| EO-85 $[H3\text{-}S8]_{2/7}$ | 12.8 | 25 | 140 ± 15 | 150 ± 16 | 72 ± 8 | 140 ± 15 | 14 ± 2 | 2.6 ± 0.2 | 60.4 ± 0.9 | 51.7 ± 0.6 |
| | | | $\varepsilon_{max} \approx 1000\%$ | | | | | | | |
| sample | O (mol %) | $T$ (°C) | $t_s(1000)$ (%) | $r(1000)$ (%) | $R(1000)$ (%) | $t_s^{I}(1000)$ (%)[a] | $t_s^{II}(1000)$ (%)[a] | $t_s^{III}(1000)$ (%)[a] | $W_{diss}^{I}$ (%)[a] | $W_{diss}^{II}$ (%)[a] |
| EO-130 $[H2\text{-}S6]_{7/15}$ | 12.4 | 25 | 382 ± 6 | 128 ± 3 | 62 ± 4 | 20.3 ± 0.8 | 3.9 ± 0.2 | 2.2 ± 0.1 | 68.8 ± 0.3 | 55.5 ± 0.4 |
| | | 60 | 900 ± 8 | 60 ± 8 | 10 ± 1 | 1.0 ± 03 | 0.2 ± 0.1 | 0.2 ± 0.1 | 65 ± 10 | 57 ± 3 |
| EO-115 $[H2\text{-}S8]_{6/12}$ | 13.1 | 25 | 333 ± 5 | 154 ± 3 | 67 ± 4 | 19.1 ± 1.6 | 3.7 ± 0.4 | 2.1 ± 0.2 | 63.8 ± 0.2 | 55.5 ± 0.4 |
| | | 60 | 600 ± 21 | 100 ± 15 | 40 ± 2 | 14 ± 9 | 1.0 ± 0.4 | 1.0 ± 0.4 | 64 ± 5 | 52 ± 1 |
| EO-107 $[H3\text{-}S9]_{4/9}$ | 12.6 | 25 | 369 ± 7 | 135 ± 3 | 63 ± 3 | 28 ± 8 | 4.2 ± 0.2 | 3 ± 1 | 67 ± 2 | 56.1 ± 0.1 |
| EO-85 $[H3\text{-}S8]_{2/7}$ | 12.8 | 25 | 378 ± 8 | 130 ± 4 | 62 ± 4 | 15.4 ± 0.6 | 3.4 ± 0.6 | 2.2 ± 0.8 | 66.4 ± 0.3 | 59.2 ± 0.4 |

[a]Superscript I, II, or III stands for first, second, or third hysteresis cycle.

block lengths and the number of blocks/chain. In particular, OBC samples with similar block length and number of blocks/chain, such as the samples EO-130 and EO-115 (Figure 2A,B) ($M_H \approx 2$ kg/mol, $M_S \approx 6-8$ kg/mol, and average number of blocks/chain ≈6−15) or the samples EO-107 and EO-85 (Figure 2A′,B′) ($M_H \approx 3$ kg/mol, $M_S \approx 8-10$ kg/mol, and average number of blocks/chain ≈2−9), and the corresponding Ei fractions, show similar mechanical properties at both 25 and 60 °C. On the other hand, the lack of strain hardening at 25 °C for the samples EO-85 (Figure 2A′) is in agreement with the low number of blocks/chain (2−8). As a consequence, strain hardening is prevented because only a loose network of chains may be formed, unable to efficiently transmit the stress at high deformations. The appearance of strain hardening at 25 °C for the corresponding Ei fraction (sample E-85Ei) (Figure 2A′) is in agreement with the fact that, compared with the corresponding unfractionated sample, the fraction EO-85Ei shows a higher molecular mass ($M_w \approx 90$ kg/mol), similar average molecular mass of the HS repeating unit ($M_{HS} \approx 12$ kg/mol), and hence a higher number of blocks/chain (3−9). However, the different mechanical behavior of the sample EO-85 and the corresponding Ei fraction may also be due to the presence of a non-negligible amount of an Es fraction in the unfractionated sample, acting as a plasticizer. It is worth noting that maintenance of a high level of ductility at 60 °C is critically dependent on the molecular characteristics of OBCs. In general, long blocks and small average number of blocks/chain, as in samples EO-107 ($[H3\text{-}S9]_{4/9}$) and EO-85 ($[H3\text{-}S8]_{2/7}$), and in the corresponding Ei fractions ($[H3\text{-}S10]_{4/9}$ and $[H3\text{-}S9]_{3/8}$), induce the formation of loose networks unable to efficiently transmit the stress, resulting in soft materials breaking at low deformations at 60 °C (Figure 2A′,B′). Chains with a high number of short blocks, instead, as in samples EO-130 ($[H2\text{-}S6]_{7/15}$) and EO-115 ($[H2\text{-}S8]_{6/12}$), and in the corresponding Ei fractions ($[H2\text{-}S6]_{10/17}$ and $[H2\text{-}S8]_{8/15}$), form tighter networks, resulting in soft elastomers at 60 °C with a high level of ductility (Figure 2A,B). Finally, the sample EO-129 and the corresponding Ei fraction ($[H3\text{-}S15]_{4/7}$ and $[H3\text{-}S15]_{6/9}$, respectively) show different molecular characteristics, and in particular a fraction of hard blocks $w_H \approx 0.15$, $M_H$ values of 2.7 kg/mol, similar to those of the samples EO-107 and EO-85, definitely higher $M_S$ values (15.5 kg/mol), and 4−9 blocks/chain. Compared with the mechanical behavior of the other OBCs, the sample EO-129 appears less strong, but it can preserve a level of ductility at 60 °C higher than that of the more crystalline samples EO-107 and EO-85 containing a higher fraction of hard blocks ($w_H \approx 0.25-26$).

It is worth noting that similar mechanical properties are obtained also for the OBC synthesized by chain shuttling technology studied in refs 4−7, 17, 24, and 25. For instance, in ref 4 the mechanical properties of a series of OBC samples characterized by octene concentration in the hard and soft blocks of 0.5 and 18.9 mol %, respectively, similar to those studied here, but an average fraction of hard blocks $w_H$ ranging from 18 to 82 wt %, are compared with those of random EO copolymers consisting of sole soft blocks ($w_H$ = 0, octene concentration ≈18.9 mol %) and sole hard blocks ($w_H$ = 100%, octene concentration ≈0.5 mol %). All samples show high ductility, and properties gradually changing from those of rigid materials up to those of elastomers. In particular, properties of rigid materials with pronounced yielding and strain hardening at high deformation occur in the case of neat hard blocks ($w_H$ = 100%) and for samples characterized by high $w_H$ content. Properties of increasingly flexible materials, with low yielding and still high strain hardening, occur in the case of samples with $w_H$ content of 27−40 wt %, whereas elastomeric properties with no pronounced yielding and scarce strain hardening are observed in the case of samples having low $w_H$ content and/or $w_H$ = 0. In our case, we explore a range of



DOI: 10.1021/acs.macromol.8b02470
Macromolecules 2019, 52, 2669−2680

properties of elastomeric type in OBC samples characterized by $w_H$ content comprised in a narrow range of 15−26 wt %, but displaying significant differences in the chain microstructure in terms of average block length and number of blocks/chain. The results of Figure 2 (Table 2) demonstrate that a fine-tuning of properties may be achieved in the polymerization step exploiting chain shuttling technology, even at fixed $w_H$ content. As a further remark we recall that the loss of strain hardening in the stress−strain curves of OBC samples stretched at high temperature has been already described.[5−7] As stated in the Introduction, this loss was attributed to activation of the crystalline $\alpha$ relaxation process.[5−7]

The elastomeric performances of the OBCs are probed by recording stress−strain curves at 25 and 60 °C during consecutive hysteresis cycles of stretch-relaxed specimens. More precisely, hysteresis cycles of consecutive stretching and relaxation recorded at 25 °C were performed on stretch-relaxed specimens prepared by stretching films obtained by compression molding at 25 °C up to $\varepsilon_{max}$ ≈500% and ≈1000% and then removing the tension still at 25 °C, whereas the hysteresis cycles recorded at 60 °C were performed on stretch-relaxed specimens prepared by stretching films obtained by compression molding at 60 °C up to $\varepsilon_{max}$ ≈500% and ≈1000% and removing the tension still at 60 °C. The tests at 60 °C were not performed for the samples EO-107 and EO-85 as they break at deformations lower than 400% at this temperature (Figure 2B′). The results of this preparative stage are reported in Table 3. Only a partial recovery of the initial dimensions is achieved for the not previously stretched (unstretched) films. In particular, at 25 °C, the values of residual deformation (tension set) are in the range of 40−140% by releasing the tension from $\varepsilon_{max}$ ≈ 500% and increase to ≈370% by releasing the tension from $\varepsilon_{max}$ ≈ 1000% (Table 3). This corresponds to a percentage of recovered strain $R(\varepsilon_{max})$ of 75−90% and ≈60% for the stretch-relaxed samples from $\varepsilon_{max}$ ≈ 500 and 1000%, respectively. For the samples EO-130, EO-129, and EO-115, the good elastomeric behavior of the unstretched films is kept also at 60 °C, but whereas for the stretch-relaxed specimens from ≈500% deformation the percentage of recovered strain $R(\varepsilon_{max})$ decreases to 50−70% (and the tension set increases), for those stretch-relaxed from ≈1000% the values of recovered strain $R(\varepsilon_{max})$ reduce to 10−40%. The highest percentage of recovered strain is achieved for the less crystalline sample EO-129 characterized by average molecular mass of the hard blocks $M_H$ of 3 kg/mol and the highest average molecular mass of soft blocks $M_S$ of 15 kg/mol in a HS repetition unit.

The mechanical cycles of the stretch-relaxed specimens recorded at 25 and 60 °C are reported in Figures 3 and 4. The values of tension set, elastic recovery, and percentage of dissipated energy measured for each cycle are reported in Table 3.

At variance with unstretched samples, the stretch-relaxed specimens show good elastomeric properties at 25 and 60 °C, in a rather wide deformation range (Figures 3 and 4). In particular, they show low values of tension set for the first cycle and negligible tension set and, hence, almost complete elastic recovery, in the successive cycles, the corresponding hysteresis curves being nearly coincident (Table 3). The percentage of dissipated energy is lower than 60% for the specimens stretch-relaxed from ≈500% deformation and slightly higher than 60% for those stretch-relaxed from ≈1000% deformation. The mechanical behavior of the stretch-relaxed specimens in the

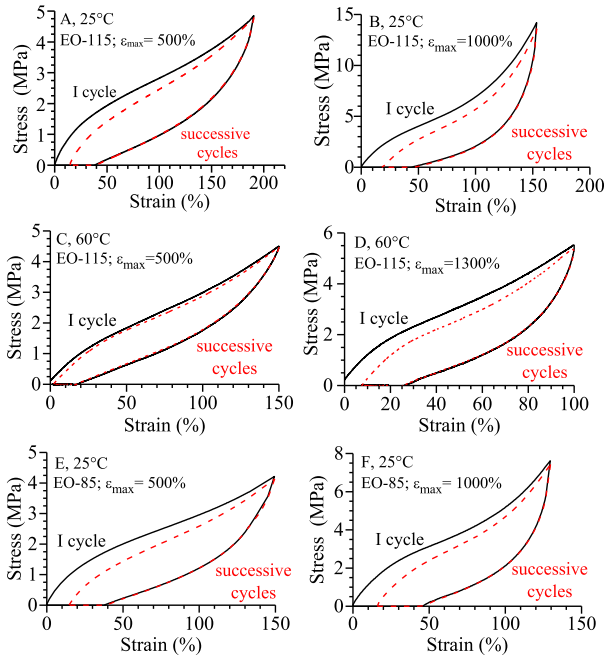


**Figure 3.** Stress−strain hysteresis cycles, consisting of consecutive stretching and relaxation steps recorded at 25 °C (A, B, E, F) and 60 °C (C, D), of stretch-relaxed specimens of the samples EO-115 (A−D) and EO-85 (E, F), obtained by stretching at 25 °C (A, B, E, F) and 60 °C (C, D) not previously stretched films (obtained by compression molding) up to the indicated values of $\varepsilon_{max}$ and then releasing the tensions. For each sample the first hysteresis cycle (solid lines) and the second cycle coincident to successive cycles (dashed lines) are reported.

cyclic mechanical tests at 25 °C of all OBCs appears equivalent (Figure 4); all of them appear having similar elastomeric performances regardless of the maximum deformation achieved in the preparative step ($\varepsilon_{max}$). The sole exception occurs for the low crystalline sample EO-129 which presents a mechanical strength lower than those of the other samples.

In particular, similar elastomeric performances occur for the samples EO-107 and EO-85 (and the corresponding Ei fractions), as their stretch-relaxed specimens show similar values for the tension set, percentage of dissipated energy (Table 3), and elastomeric performance in a deformation range of 130−170%, in agreement with the similar molecular characteristics, namely average block length ($M_H$ ≈ 3 kg/mol, $M_S$ ≈ 8−9 kg/mol) and number of blocks/chain (2−9). The elastomeric performances of the samples EO-130 and EO-115 (and the corresponding Ei fractions) also appear similar (Figure 4), as also in this case they have similar average block length ($M_H$ ≈ 2 kg/mol, $M_S$ ≈ 6−8 kg/mol) and number of blocks/chain (6−17).

At 60 °C, the unstretched films of these samples show low values of the percentage of recovered strain $R(\varepsilon_{max})$, especially after releasing the tension from ≈1000% deformation ($R(1000)$ = 10−40%), which results in elastomeric performances in a narrower deformation range.

The structural transformations occurring during deformation and after releasing the tension at room temperature are probed by performing X-ray fiber diffraction analysis of stretched samples. As an example, the X-ray fiber diffraction patterns of the samples EO-130 and EO-85 are reported in Figure 5. Starting from the unstretched films, which show the 110 and 200 reflections of the orthorhombic form of PE at $2\theta$ ≈ 21°



DOI: 10.1021/acs.macromol.8b02470
Macromolecules 2019, 52, 2669−2680

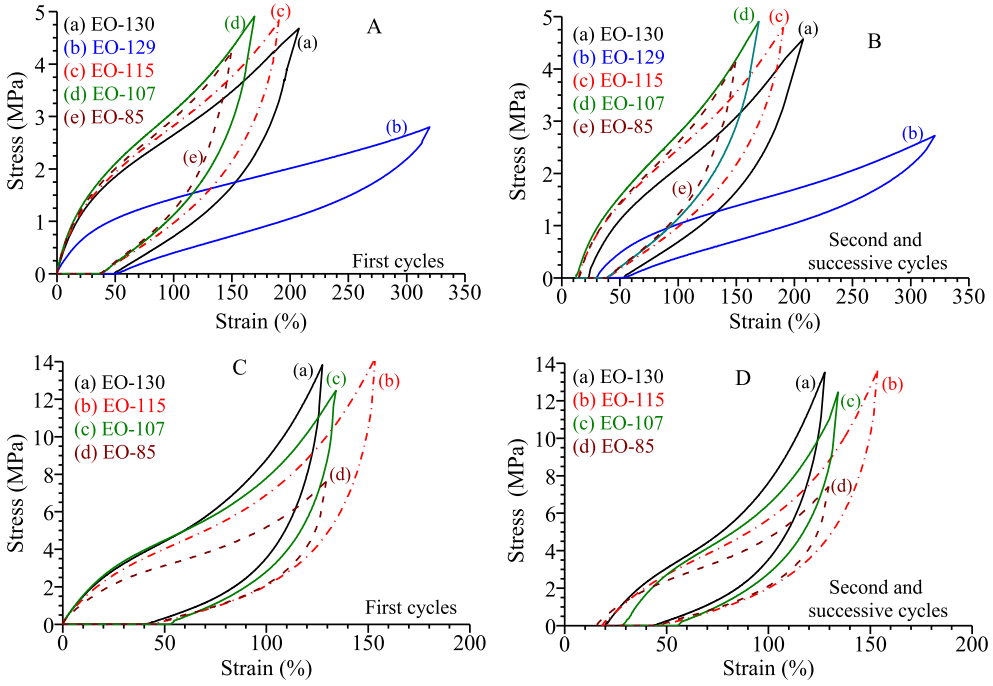


**Figure 4.** Stress−strain hysteresis cycles, consisting of consecutive stretching and relaxation steps recorded at 25 °C, of stretch-relaxed specimens of the indicated OBCs samples, obtained by stretching at 25 °C films obtained by compression molding up to deformations $\varepsilon_{max} \approx 500$ (A, B) and 1000% (C, D) and then releasing the tension. The stress−strain curves recorded during the second and successive cycles (B, D) after the first one (A, C) are coincident.

and 24°, overlying the amorphous halo centered at $2\theta \approx 19°$ (Figure 5A,A′,D,D′), the stretching at 800% strain induces not only orientation of the crystals, as indicated by the polarization of the 110 and 200 reflections on the equator, but also orientation of the amorphous phase (Figure 5B,B′,E,E′).

More precisely, besides the amorphous halo of the main amorphous component, which is not oriented, a second halo strongly polarized on the equator appears (Figure 5B,E). Simultaneously, the corresponding equatorial profiles (Figure 5B′,E′) reveal decrease in the relative intensity of 110 and 200 reflections and no shift in $2\theta$ position, increase in the relative intensity of the amorphous halo and shift of its maximum to $2\theta \approx 20°$. Upon release of the tension (Figure 5C,C′,F,F′), the orientation of PE crystals is largely lost, and the equatorial polarization of the amorphous halo disappears. In particular, in the equatorial profiles (Figure 5C′,F′) the relative intensity of 110 and 200 reflections of PE increases and that of the amorphous halo decreases, while the amorphous maximum returns back to its pristine $2\theta$ position of ≈19°. It is worth noting that the polarization of the amorphous phase on the equator is not related to the stress-induced martensitic transformation of the orthorhombic form of PE in the monoclinic form. Indeed, the main reflection of the monoclinic form (001, *b*-chain axis) of PE occurs at $2\theta \approx 19$ °C, not at $2\theta \approx 20°$ as instead observed in our case.[31]

These texture/structure changes are reversible. In consecutive mechanical cycles of stretching and release of the tension, orientation/disorientation of the crystals occurs, accomplished by the orientation/disorientation of the amorphous phase, while reversible shift of the $2\theta$ position of the amorphous maximum on the equator also occurs. These reversible changes are common to all OBC samples and are due to their peculiar architecture.

The stretching at high deformations, indeed, induces breaking of the initial spherulitic morphology[28] and fragmentation of the crystals. The crystals tend to become oriented with the chain axes parallel to the stretching direction, obtaining oriented fibers. This morphological transformation is irreversible and explains the low elastic performance of the initial unstretched films.

The mechanism underlaying the texture/structure transformations of stretch-relaxed specimens of OBC is sketched in Figure 6. By the effect of stretching, the simultaneous decrease of the relative intensity of 110 and 200 reflections of the PE crystals and increase of intensity of the amorphous halo on the equator are probably due to partial (mechanical) melting of the crystals and transformation into an oriented amorphous phase (Figure 6B). Therefore, the so-formed new amorphous phase involves segments belonging to hard blocks and in part also the amorphous phase placed in between the crystals in more constrained regions. The chains belonging to the constrained amorphous phase, during deformation, experience compressive forces transversal to the stretching directions, resulting in a decrease of the average interchain distance (Figure 6B), as indicated by the shift of the $2\theta$ position of the amorphous halo on the equator toward higher values. Upon release of the tension, the orientation of the crystals is lost and the oriented amorphous phase relaxes, up to recrystallize again, inducing increase in the relative intensity of crystalline reflections and decrease of intensity of the amorphous phase (Figure 6A).

These texture/structure transformations occurring in stretch-relaxed specimens are reversible and are accomplished by complete elastic recovery. The key for understanding the orientation/disorientation mechanism of OBCs stems from their statistical multiblock architecture and the tendency of hard blocks to crystallize in separated domains. Because


DOI: 10.1021/acs.macromol.8b02470
*Macromolecules* 2019, 52, 2669−2680

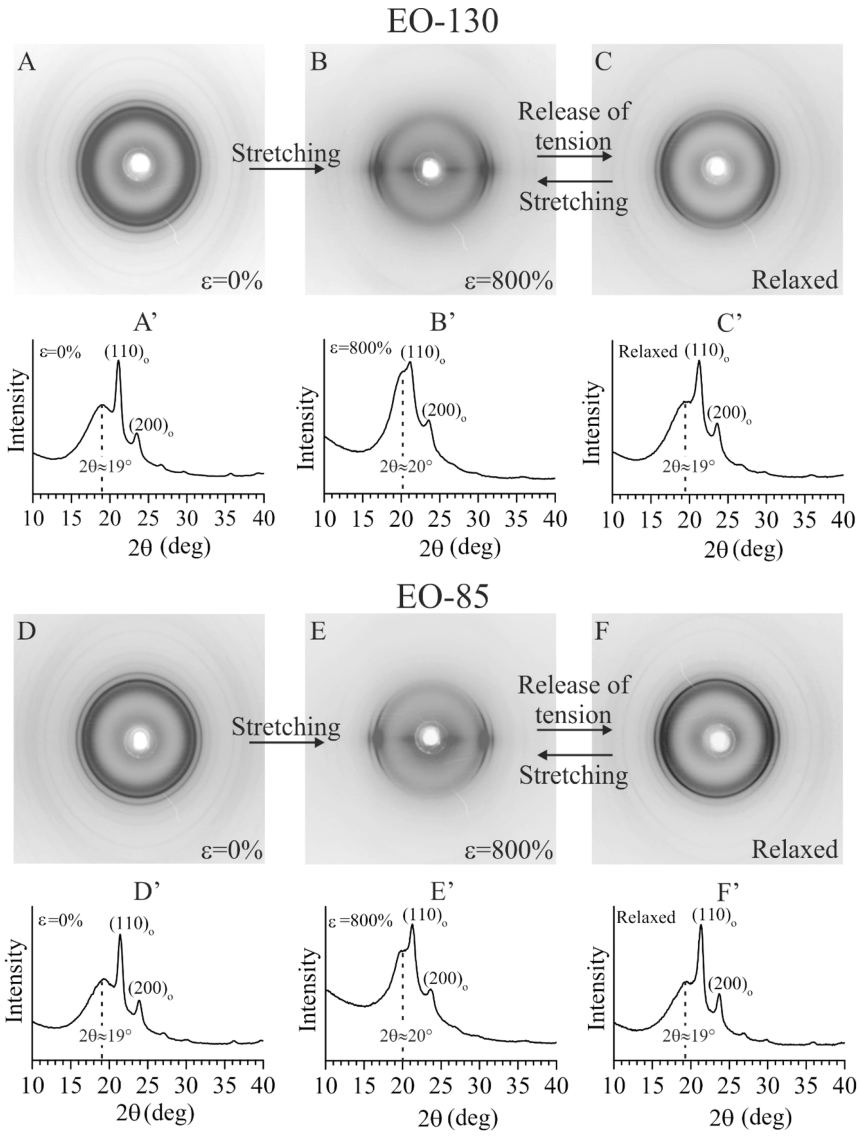


**Figure 5.** X-ray fiber diffraction patterns (A−F) and corresponding equatorial profiles (A′−F′) of films of the OBC samples EO-130 and EO-85 before deformation (A, A′, D, D′), after stretching at 800% deformation (B, B′, E, E′), and successive release of the tension (C, C′, F, F′). The $(110)_o$ and $(200)_o$ reflections of the orthorhombic form of polyethylene are indicated in (A′−F′). The orientation/disorientation of the crystals and amorphous phase in (B, C) and (E, F) is reversible in consecutive cycles of stretching and release of the tension, while the samples show elastomeric properties. The dashed lines indicate the position of the maximum for the amorphous halo on the equator.

crystals are formed in separated domains populated by hard blocks,[28,32] the orientation/disorientation of the crystals is facilitated by the high level of compliance of the amorphous matrix populated by soft blocks, in which the hard domains are embedded.

## CONCLUSIONS

The mechanical properties and the structural transformations occurring during deformation of ethylene/1-octene multiblock copolymers, obtained by chain shuttling technology, are investigated. The analysis is performed on the unfractionated samples and after removal of an almost completely amorphous fraction soluble in boiling diethyl ether, which represents only the 6−14 wt % of the total.

The samples are characterized by hard and soft blocks with identical concentration of comonomeric units, equal to ≈0.5 and ≈18.9 mol %, respectively, small differences in molecular mass and fractional content of hard blocks, and subtle differences in the melting and crystallization properties but remarkable differences for the mechanical properties. We highlight that the mechanical properties of these systems reflect the differences in the average molecular mass of soft and hard blocks and number of blocks/chain, even though the octene concentration is the same.

At 25 °C all samples show high ductility and strain hardening at high deformations. The sole exception is observed for the unfractionated sample EO-85 with relatively high block length and low number of blocks/chain, even though, after removal of the Es fraction, the corresponding Ei fraction displays strain hardening, as all the other samples. At 60 °C the samples become softer, do not show strain hardening, and maintain high ductility. Different behavior has been observed for the samples EO-85 and EO-107, which present a high length of blocks and the lowest number of blocks/chain and experience breaking at low deformations. In general, the mechanical properties of Ei fraction are similar to those of


DOI: 10.1021/acs.macromol.8b02470
Macromolecules 2019, 52, 2669−2680

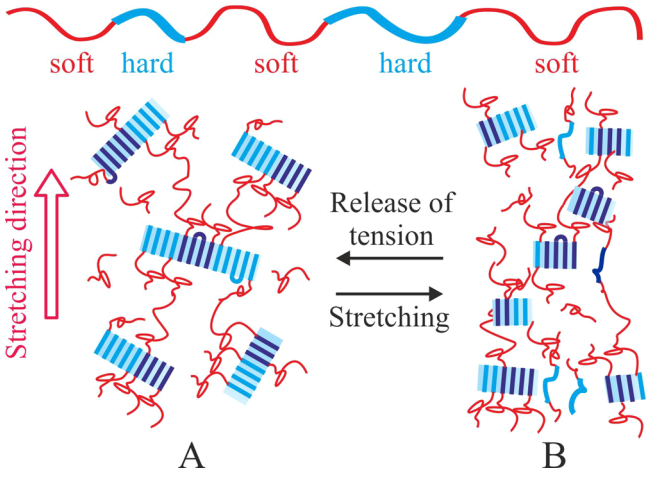


**Figure 6.** Possible mechanism associated with the elastic recovery of OBC specimens by effect of stretching (B) and release of the tension (A). Stretching induces orientation of the crystals and mechanical melting, with consequent reduction of the lateral size of the fringed micelle like crystals formed by the hard blocks. A new amorphous phase is formed by the segments belonging to the hard blocks which remains entrapped in between the residual crystals and assumes an elongated conformation parallel to the stretching direction. The chain in the new amorphous phase also experience compressive forces in the transversal direction, resulting in a decrease of the average interchain distance (B). Upon release of the tension, the orientation of the crystals and amorphous phase is lost, and the hard blocks recrystallize on the pristine crystals. For clarity, the entangled amorphous phase is not drawn, and only some tie molecules are indicated.

unfractionated samples, indicating that the presence of the Es fraction plays little or no effect in the deformation behavior.

The initial unstretched films show only partial elastic recovery after stretching at high deformation and successive release of the tension. The percentage of recovered strain depends on the maximum deformation achieved in the stretching step $\varepsilon_{max}$ and temperature. At 25 °C, the recovered strain is higher than 70% by releasing the tension from $\varepsilon_{max}$ = 500% and remains high even at 60 °C. However, the recovered strain after releasing the tension from higher deformation of $\varepsilon_{max}$ = 1000% decreases to 60% at 25 °C and becomes lower than 40% at 60 °C.

The stretch-relaxed specimens of OBCs obtained by stretching the initial unstretched films up to 500 and 1000% and releasing the tension, instead, show good elastomeric properties at 25 °C in a deformation range higher than 100%. However, at 60 °C good elastic properties of these specimens are maintained only for the samples EO-130 and EO-115 characterized by short blocks and high number of blocks/chain, the corresponding Ei fractions, and the samples EO-129 and EO-129Ei with the lowest fractional content of hard blocks and the highest length of soft blocks.

The fiber diffraction analysis of OBCs reveals a singular behavior, consisting in the orientation not only of the crystals but also of the amorphous phase. The orientation of amorphous phase essentially occurs for the new amorphous phase formed by effect of partial mechanical melting of the crystals during deformation. The resultant new amorphous phase involves segments belonging to hard blocks, extracted from the pristine crystals. As these chains tend to assume elongated conformations in the stretching direction, compressive forces are also involved reducing the relative distance between chain axes in the transversal direction. The above transformations are reversible, and the release of the tension is accomplished by recrystallization and disorientation of the crystals and of the amorphous phase.

The reversible phenomena occurring in cyclic steps of stretching followed by release of the tension of OBCs, that is, melting/recrystallization coupled with the orientation/disorientation of the crystals and of the amorphous phase, and the reduction/increase of the interchain distance of the amorphous coils, are associated with the peculiar molecular structure of these systems, involving the crystallization of hard blocks in separated domains, forming lamellar crystals of small lateral size, floating in the compliant amorphous matrix populated by the longer soft blocks.

Therefore, the formation of tight or loose networks with good or poor mechanical properties at 25 °C and at higher temperature is critically dependent on the length of hard and soft blocks, as fixed in the synthetic step, according to the chain shuttling process.

## AUTHOR INFORMATION


### Corresponding Author

*E-mail finizia.auriemma@unina.it.

### ORCID

Finizia Auriemma: 0000-0003-4604-2057
Claudio De Rosa: 0000-0002-5375-7475
Miriam Scoti: 0000-0001-9225-1509
Rocco Di Girolamo: 0000-0001-8815-2997
Anna Malafronte: 0000-0002-7854-5823
Incoronata Tritto: 0000-0001-8364-4298


### Notes

The authors declare no competing financial interest.

## ACKNOWLEDGMENTS

Financial support from the CARIPLO Foundation (20130721-Crystalline Elastomers) and from the University of Napoli (project Ricerca di Ateneo) is gratefully acknowledged.

## REFERENCES


(1) Arriola, D. J.; Carnahan, E. M.; Hustad, P. D.; Kuhlman, R. L.; Wenzel, T. T. Catalytic production of olefin block copolymers via chain shuttling polymerization. *Science* **2006**, *312*, 714−719.

(2) https://www.dow.com/elastomers/products/infuse.html.

(3) Wenzel, T. T.; Arriola, D. J.; Carnahan, E. M.; Hustad, P. D.; Kuhlman, R. L. Chain Shuttling Catalysis and Olefin Block Copolymers (OBCs). In *Metal Catalysts in Olefin Polymerization. Topics in Organometallic Chemistry*; Guan, Z., Ed.; Springer: Berlin, 2009; Vol. *26*.

(4) Wang, H. P.; Khariwala, D. U.; Cheung, W.; Chum, S. P.; Hiltner, A.; Baer, E. Characterization of Some New Olefinic Block Copolymers. *Macromolecules* **2007**, *40*, 2852−2862.

(5) Wang, H. P.; Chum, S. P.; Hiltner, A.; Baer, E. Comparing elastomeric behavior of block and random ethylene−octene copolymers. *J. Appl. Polym. Sci.* **2009**, *113*, 3236−3244.

(6) Zuo, F.; Burger, C.; Chen, X. M.; Mao, Y. M.; Hsiao, B. S.; Chen, H. Y.; Marchand, G. R.; Lai, S. Y.; Chiu, D. An in Situ X-ray Structural Study of Olefin Block and Random Copolymers under Uniaxial Deformation. *Macromolecules* **2010**, *43*, 1922−1929.

(7) Zuo, F.; Mao, Y. M.; Li, X. W.; Burger, C.; Hsiao, B. S.; Chen, H. Y.; Marchand, G. R. Effects of Block Architecture on Structure and Mechanical Properties of Olefin Block Copolymers under Uniaxial Deformation. *Macromolecules* **2011**, *44*, 3670−3673.

(8) Hustad, P. D.; Kuhlman, R. L.; Carnahan, E. M.; Wenzel, T. T.; Arriola, D. J. An Exploration of the Effects of Reversibility in Chain




DOI: 10.1021/acs.macromol.8b02470
*Macromolecules* 2019, 52, 2669−2680

Transfer to Metal in Olefin Polymerization. *Macromolecules* **2008**, *41*, 4081−4089.
(9) Kuhlman, R. L.; Wenzel, T. T. Investigations of Chain Shuttling Olefin Polymerization Using Deuterium Labeling. *Macromolecules* **2008**, *41*, 4090−4094.
(10) Zhang, M.; Carnahan, E. M.; Karjala, T. W.; Jain, P. Theoretical Analysis of the Copolymer Composition Equation in Chain Shuttling Copolymerization. *Macromolecules* **2009**, *42*, 8013−8016.
(11) Zhang, M.; Karjala, T. W.; Jain, P. Modeling of $\alpha$-Olefin Copolymerization with Chain-Shuttling Chemistry Using Dual Catalysts in Stirred-Tank Reactors: Molecular Weight Distributions and Copolymer Composition. *Ind. Eng. Chem. Res.* **2010**, *49*, 8135−8146.
(12) Kuhlman, R. L.; Klosin, J. Tuning Block Compositions of Polyethylene Multi-Block Copolymers by Catalyst Selection. *Macromolecules* **2010**, *43*, 7903−7904.
(13) Zhang, M.; Karjala, T. W.; Jain, P.; Villa, C. Theoretical Modeling of Average Block Structure in Chain-Shuttling $\alpha$−Olefin Copolymerization Using Dual Catalysts. *Macromolecules* **2013**, *46*, 4847−4853.
(14) Mohammadi, Y.; Ahmadi, M.; Saeb, M. R.; Khorasani, M. M.; Yang, P.; Stadler, F. J. A Detailed Model on Kinetics and Microstructure Evolution during Copolymerization of Ethylene and 1-Octene: From Coordinative Chain Transfer to Chain Shuttling Polymerization. *Macromolecules* **2014**, *47*, 4778−4789.
(15) Saeb, M. R.; Khorasani, M. M.; Ahmadi, M.; Mohammadi, Y.; Stadler, F. J. A unified picture of hard-soft segmental development along olefin chain shuttling copolymerization. *Polymer* **2015**, *76*, 245−253.
(16) Khariwala, D. U.; Taha, A.; Chum, S. P.; Hiltner, A.; Baer, E. Crystallization kinetics of some new olefinic block copolymers. *Polymer* **2008**, *49*, 1365−1375.
(17) Wang, H. P.; Chum, S. P.; Hiltner, A.; Baer, E. Deformation of elastomeric polyolefin spherulites. *J. Polym. Sci., Part B: Polym. Phys.* **2009**, *47*, 1313−1330.
(18) Li, S.; Register, R. A.; Weinhold, J. D.; Landes, B. G. Melt and Solid-State Structures of Polydisperse Polyolefin Multiblock Copolymers. *Macromolecules* **2012**, *45*, 5773−5781.
(19) Park, H. E.; Dealy, J. M.; Marchand, G. R.; Wang, J. A.; Li, S.; Register, R. A. Rheology and Structure of Molten, Olefin Multiblock Copolymers. *Macromolecules* **2010**, *43*, 6789−6799.
(20) Liu, G. M.; Guan, Y.; Wen, T.; Wang, X.; Zhang, X. Q.; Wang, D. J.; Li, J.; Loos, X. H.; Chen, H. Y.; Walton, K.; Marchand, G. Effect of mesophase separation and crystallization on the elastomeric behavior of olefin multi-block copolymers. *Polymer* **2011**, *52*, 5221.
(21) Wen, T.; Liu, G. M.; Zhou, Y.; Zhang, X. Q.; Wang, F. S.; Chen, H. Y.; Loos, J.; Wang, D. J. Epitaxy-Induced Crystallization of Olefin Block Copolymers. *Macromolecules* **2012**, *45*, 5979−5985.
(22) Jin, J.; Du, J. A.; Xia, Q. H.; Liang, Y. R.; Han, C. C. Effect of Mesophase Separation on the Crystallization Behavior of Olefin Block Copolymers. *Macromolecules* **2010**, *43*, 10554−10559.
(23) Tong, Z. Z.; Huang, J.; Zhou, B.; Xu, J. T.; Fan, Z. Q. Chain microstructure, crystallization, and morphology of olefinic blocky copolymers. *Macromol. Chem. Phys.* **2013**, *214*, 605−613.
(24) Tong, Z. Z.; Zhou, B.; Huang, J.; Xu, J. T.; Fan, Z. Q. Regulation of Crystallization Kinetics, Morphology, and Mechanical Properties of Olefinic Blocky Copolymers. *Macromolecules* **2014**, *47*, 333−346.
(25) Zhao, Y.; Zhu, Y.; Sui, G.; Chen, F.; Zhang, F.; Fu, Q. The effect of hard block content on the orientation and mechanical properties of olefin block copolymer films as obtained *via* melt stretching. *RSC Adv.* **2015**, *5*, 82535−82543.
(26) Hustad, P. D.; Marchand, G. R.; Garcia-Meitin, E. I.; Roberts, P. L.; Weinhold, J. D. Photonic Polyethylene from Self-Assembled Mesophases of Polydisperse Olefin Block Copolymers. *Macromolecules* **2009**, *42*, 3788−379.
(27) Vittoria, A.; Busico, V.; Cannavacciuolo, F. D.; Cipullo, R. Molecular Kinetic Study of "Chain Shuttling" Olefin Copolymerization. *ACS Catal.* **2018**, *8*, 5051−5061.
(28) Auriemma, F.; De Rosa, C.; Scoti, M.; Di Girolamo, R.; Malafronte, A.; Talarico, G.; Carnahan, E. Unveiling the Molecular Structure of Ethylene/1-Octene Multi-block Copolymers from Chain Shuttling Technology. *Polymer* **2018**, *154*, 298−304.
(29) Voigt-Martin, I. G.; Fischer, E. W.; Mandelkern, L. Morphology of melt-crystallized linear polyethylene fractions and its dependence on molecular weight and crystallization temperature. *J. Polym. Sci., Polym. Phys. Ed.* **1980**, *18*, 2347−2367.
(30) Robelin-Souffache, E.; Rault, J. Origin of the long period and crystallinity in quenched semicrystalline polymers. 1. *Macromolecules* **1989**, *22*, 3581−3594.
(31) Russell, K. E.; Hunter, B. K.; Heyding, R. D. Monoclinic polyethylene revisited. *Polymer* **1997**, *38*, 1409−1414.
(32) Auriemma, F.; De Rosa, C.; Scoti, M.; Di Girolamo, R.; Malafronte, A.; Galotto Galotto, N. Structural Investigation at Nanometric Length Scale of Ethylene/1-Octene Multi-block Copolymers from Chain Shuttling Technology. DOI: 10.1021/acs.macromol.8b01947.



DOI: 10.1021/acs.macromol.8b02470
*Macromolecules* 2019, 52, 2669−2680